The effects of noise in cardiac diffusion tensor imaging and the benefits of averaging complex data

Andrew D Scott[1,2], Sonia Nielles-Vallespin[1,3], Pedro FADC Ferreira[1,2], Laura-Ann McGill[1,2], Dudley J Pennell[1,2], David N Firmin[1,2]

1. Cardiovascular Biomedical Research Unit, The Royal Brompton and Harefield NHS Foundation Trust and Imperial College London, UK.
2. National Heart and Lung Institute, Imperial College, London, UK.
3. National Heart Lung and Blood Institute, National Institutes for Health, Bethesda, Maryland, USA.

Corresponding Author:

Dr Andrew D Scott, Cardiovascular Biomedical Research Unit, The Royal Brompton Hospital, Sydney Street, London, SW3 6NP. a.scott@rbht.nhs.uk

Key words: MRI, DTI, cardiac, noise, simulations, averaging.

Word count: 8,104 (Introduction – document end)

Graphical abstract

Image noise causes an over-estimation of mean diffusivity (MD) and fractional anisotropy (FA) and under-estimation of E2A (relating to sheetlet orientation) at low b-values and an under-estimation FA, MD and E2A at high b-values. Simulations demonstrate that the noise effects at high b-values can be mitigated by averaging complex rather than magnitude data. An algorithm for subtracting the motion induced image phase is implemented which allows complex averaging *in vivo* and compensation for the noise floor effects at high b-values.

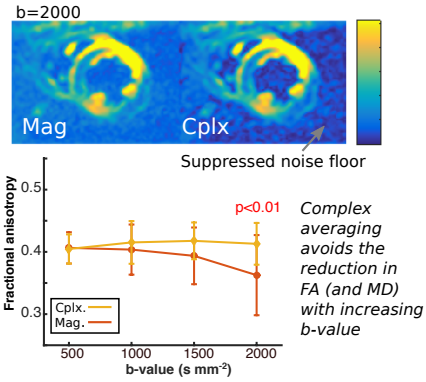

Abstract Summary:

There is growing interest in cardiac diffusion tensor imaging (cDTI), but unlike other diffusion MRI applications, there has been little investigation of the effects of noise on the parameters typically derived. One method of mitigating noise floor effects when there are multiple image averages, as in cDTI, is to average the complex rather than the magnitude data, but the phase contains contributions from bulk motion, which must be removed first.

The effects of noise on mean diffusivity (MD), fractional anisotropy (FA), helical angle (HA) and the absolute secondary eigenvector angle (E2A) were simulated with various diffusion weightings (b-values). The effect of averaging complex versus magnitude images was investigated.

In-vivo cDTI was performed in 10 healthy subjects with b=500, 1000, 1500 and 2000smm^{-2}. A technique for removing the motion-induced component of image phase present *in-vivo* was implemented by subtracting a low-resolution copy of the phase from the original images before averaging the complex images. MD, FA, E2A and the transmural gradient in HA were compared for un-averaged, magnitude and complex averaged reconstructions.

Simulations demonstrated over-estimation of FA and MD at low b-values and under-estimation at high b-values. The transition is relatively SNR independent and occurs at a higher b-value for FA (b=1000-1250smm^{-2}) than MD (b≈250smm^{-2}). E2A is under-estimated at low and high b-values with a transition at b≈1000smm^{-2}, whereas the bias in HA is comparatively small. The under-estimation of FA and MD at high b-values is caused by noise floor effects which can be mitigated by averaging the complex data.

Understanding the parameters of interest and the effects of noise informs the selection of the optimal b-values. When complex data is available it should be used to maximise the benefit from acquiring multiple averages. Combining complex data is also a valuable step towards segmented acquisitions.

List of abbreviations

DTI – diffusion tensor imaging

cDTI – cardiac DTI

SNR – signal to noise ratio

HA – helical angle

FA – fractional anisotropy

MD – mean diffusivity

EPI – echo planar imaging

STEAM-EPI – stimulated echo acquisition mode – EPI

E2A – absolute angle of the second eigenvector of the diffusion tensor

S_0 – signal intensity with diffusion encoding

b_{main} – diffusion weighting of the images with the higher of the two diffusion weightings used to reconstruct the tensor

b_{ref} – diffusion weighting of the reference images (often referred to as b_0 images), i.e. the smaller of the two diffusion weightings

G – diffusion gradient strength

T_{SS} – duration of the slice select and accompanying rephasing gradient

T_{EPI} – duration of the echo planar imaging echo train

RR – RR interval (period) of the cardiac cycle

N_A – number of image averages

TE – echo time

TR – repetition time

FOV – field of view

HAg – transmural helical angle gradient

HA-R^2 – coefficient of determination (R^2) of the linear regression of the HAg

ANOVA – analysis of variation

GRAPPA – generalised autocalibrating partially parallel acquisitions

SENSE – sensitivity encoding

Introduction

The unique ability of cardiac diffusion tensor imaging (cDTI) to provide non-invasive information on myocardial microstructure *in vivo* has led to a number of recent technical developments(1,2,3,4) and insights into normal and diseased structure and function(5,6). Yet a number of uncertainties and controversies remain, including the effects of mixing time(7), strain(8) and noise. While the first two of these have partial solutions(7,8,9) and the effects of noise were described in general(10,11), there is uncertainty regarding the specific effects of noise on the parameters typically derived from cDTI at the signal to noise ratios (SNR) achieved. Further insights may partially explain the differences between parameters reported in the literature(12).

The structure of myocardial tissue is inherently very different from that of the central nervous system. While the neuronal bundles forming white matter have a cylindrical symmetry, myocardial tissue is fully orthotropic. As a result parameters such as radial diffusivity are less frequently quoted in the heart and the interpretation of tractography is less clear cut. However, the known progression from a left-handed helical arrangement of cardiomyocytes in the epicardium, through a circumferential orientation in the mesocardium to a right-handed helical arrangement in the endocardium(13) means that the helical angle (HA) is a widely quoted parameter. Diffusion of water molecules within the cleavage planes between functional units of cardiomyocytes known as sheetlets may be reflected in the secondary eigenvalue/vector of the diffusion tensor which rotates between systole and diastole(14,15). Recently we have shown that the mobility of the absolute value of the angle of the secondary eigenvector (E2A) between systole and diastole is substantially impaired in patients with hypertrophic cardiomyopathy(6).

Fractional anisotropy (FA) and mean diffusivity (MD) are well established descriptors of the diffusion tensor that are widely used in studies of both cardiac and neurological diffusion. Increasing noise is typically thought to result in an increasing under-estimation of MD(11). Jones and Basser (11) described the transition from a low b_{main} (the higher of the two b-values used) regime, where the effect of noise was to increase FA via eigenvalue repulsion, to a high b_{main} regime, where the noise floor limits the value of the primary eigenvalue and, hence the FA (so-called squashing the

peanut). The majority of *in-vivo* cDTI studies have been performed at low b_{main} values when compared to those typically used in neurological studies. However, the location of the transition from low to high b_{main} regimes is uncertain in cDTI and the effects of noise on HA and the secondary eigenvector have not been described.

cDTI techniques typically acquire several averages to reduce the effects of noise. However, any difference in tissue position between the diffusion gradients is encoded in the image phase. Differences in phase between averages result in signal cancellation when complex data is averaged and therefore, magnitude averaging is used. Magnitude averaging improves SNR in regions of high signal but does not reduce the background signal (the noise floor). Some brain DTI studies have estimated the motion-induced phase based on the assumption that the motion induced phase varies gradually across the image and subtracted it(16) before averaging the complex data. These methods have not been demonstrated in the heart until now and the reliance of cDTI on averaging suggests that it may be a suitable application. Correction of the motion-induced phase is also a vital step towards a segmented cDTI acquisition which would permit higher resolution studies.

In this work we simulate the effects of noise on FA, MD, HA and the second eigenvector using a cDTI specific model. We implement a complex averaging algorithm for cDTI data based on the slowly varying approximation of motion-induced phase and demonstrate the b_{main} regime in which it is beneficial using both simulations and in *in-vivo* imaging.

Experimental

Simulations

Numerical simulations were performed in order to demonstrate the effects of noise on cDTI acquisitions and determine the b-value and SNR regime in which averaging complex data is worthwhile. A numerical phantom was created in Matlab (Mathworks, Natick, MA) based on systolic mid-ventricular short-axis cDTI data from a previous study(2). The data were acquired with a stimulated-echo – echo-planar imaging sequence (STEAM-EPI)(1,17), with b_{main}=750 smm^{-2} (8 averages) and the reference b-value, b_{ref}=150smm^{-2} (1 average). The simulated image contained a left ventricle defined by an annulus with a thickness of 10 reconstructed pixels. HA(17) varied

linearly from -60° to +60° epi- to endocardium, MD=0.9x10-3 mm^2s^{-1}, FA=0.42 and the tensor mode(18) was 0 (eigenvalues [1.3, 0.9, 0.5]x$10^{-3}mm^2s^{-1}$) uniformly. As in (6), E2A was defined as the absolute value of the angle between the radial direction and second eigenvector of the diffusion tensor projected into the radial – cross-myocyte plane. The cross-myocyte direction is perpendicular to the radial direction and the projection of the primary eigenvector into the circumferential–longitudinal plane. E2A is thought to represent the mean orientation of the sheetlet/shear layer planes (6) in the myocardium and 60° was used here globally. These parameters were used to create a simulated diffusion tensor at every pixel.

Simulated diffusion encoded images were created using 6 diffusion encoding directions (in (x,y,z) co-ordinates (1,0,1), (1,0,-1), (0,1,1), (0,1,-1), (1,1,0), (-1,1,0)) with an x-y imaging plane and a uniform signal intensity without diffusion encoding (S_0). The diffusion weighting for each direction and average was scaled by a normally distributed random value to account for the beat-to-beat variations in RR interval that scale the b-value proportionately. The simulated images (6 directions + reference, b_{ref}=0) were scaled for T2 decay (assuming T2=50ms) according to the minimum TE required for the corresponding b_{main}. The TE for the STEAM sequence is the time between the first and second RF pulses plus that between the third RF pulse and the centre of k-space (these times must be equal). Assuming a linear phase encode scheme, the time between the third RF pulse and the echo determines TE, giving: $TE = T_{SS} + T_{EPI} + 2\left(\frac{1}{\gamma G}\right) \cdot \sqrt{\frac{b_{main}}{RR}}$, where T_{SS} and T_{EPI} are the durations of the slice select gradient and rephasing gradient for the third RF pulse (4ms) and EPI echo train (13ms) respectively, *G* is the diffusion gradient strength (0.04Tm^{-1}) and *RR* is the RR interval (1000ms fixed). The third term in this equation is twice the diffusion gradient duration neglecting ramp times and assuming that *RR* was much greater than the diffusion gradient duration. T2* decay during the echo train was not included in the simulation.

The images were Fourier transformed and noise was added to the complex k-space data by adding a random number with an overall Gaussian distribution to the magnitude and phase at each pixel. To simulate the effects of the zero-filling performed for *in-vivo* acquisitions, the data was masked to zero the outer regions of k-space, halving the spatial resolution. These steps were repeated N_A times to

simulate the effects of collecting N_A cDTI signal averages. In order to most closely match the *in-vivo* acquisitions, the SNR was varied between 5.9 and 21 (in the b_{ref}=0 images before averaging at a TE sufficient to achieve b=750smm^{-2}) by changing the standard deviation of the Gaussian noise.

The simulated data was processed using modified versions of the tools developed for *in-vivo* cDTI data in previous studies(2,5,6). The tensor was calculated using a linear least squares inversion. Maps of HA, MD, FA and E2A were generated. The mean signed difference (bias, relating to accuracy) and the mean absolute difference (precision) was calculated between the results of each simulation and the ground truth.

The mean SNR in the left ventricle (before averaging) was measured in the b_{ref}=0 images as the ratio between the mean signal and the standard deviation between signal averages for every pixel(1). Due to the scaling used to account for changes in TE at different b_{main} values, the SNR in the b_{ref}=0 images varies with different b_{main} values for a given level of added noise. The values quoted in this work are those for the b_{ref}=0 images for which the TE is the minimum required to achieve b_{main}=750smm^{-2}.

Simulations were performed with the following parameters: b_{main}=50, 100, 150, 250 – 3000smm^{-2} in steps of 250 smm^{-2}; 12 averages; b_{ref}=0 (6 averages); 9 added noise levels; a simulated standard deviation in the RR interval of 65ms (based on heart rate variations in previously acquired data (2)) and an average RR interval of 1s; and either magnitude averaging, beat-to-beat correction (including each average and direction in the matrix inversion with the corresponding simulated heart rate corrected b-value) or complex averaging. As there was no motion in the simulated data, phase correction was not performed for complex averaging and the mean of the complex data was taken before calculating the magnitude and processing as for magnitude averaged data.

In order to demonstrate the performance of the 3 processing methods (magnitude averaging, beat-to-beat correction and complex averaging) in response to variations in other parameters the simulations were repeated with a fixed SNR=11 and other parameters as above. The effect of increasing the diffusion weighting of the

reference images, which may be used to reduce the contribution of microvascular perfusion (2,3) was investigated by increasing b_{ref} to 150smm^{-2}. Heart rate variation was tested by using a simulated standard deviation in the RR-interval of 0, 35 and 65ms. Signal averaging was investigated using 4, 8 and 12 averages. The influence of the MD on the results was simulated by scaling the input diffusion tensor to give MD values encompassing those reported in previous studies (19) 0.5, 0.9 (2) and 2.4 x10^{-3}smm^{-2} (20). Finally, changes in FA (covering values reported in the literature) were simulated with eigenvalues/FA of [1.1, 0.9, 0.7]/0.22 (21,22), [1.3, 0.9, 0.5]/0.42 (2) and [1.7, 0.9, 0.1]/0.72 (19,23) whilst MD was maintained at 0.9x10^{-3}smm^{-2}.

In-vivo imaging

Ten healthy subjects (6 male, median age 33, range 22-59 years) were recruited in accordance with ethical approval. Imaging was performed on a Siemens Skyra 3T scanner (Siemens Healthcare, Erlangen Germany) with maximum gradients and slew rate of 0.045Tm^{-1} and 180Tm^{-1}s^{-1} using an 18 element anterior coil and 8-12 elements of a posterior spine coil. A single slice mid-ventricular short-axis systolic cDTI acquisition was planned as in previous work(2). Breath-hold cDTI was performed using STEAM-EPI with monopolar diffusion encoding(1,17). Spatial resolution was 2.8x2.8mm^2 (1.4x1.4mm^2 via zero-filling), 8mm slice thickness, reduced phase field of view (FOV) via zonal excitation, FOV 360 x 135mm^2, echo train length 24, repetition time 2RR-intervals (1RR-interval of T1 recovery). Each breath hold was 18RR-intervals, consisting of 2RR-intervals for each of: EPI phase correction lines; parallel imaging reference data; a reference b_{ref}=34smm^{-2} image; and each of the 6 diffusion encoding directions. Factor 2 SENSE parallel imaging was used and both magnitude and phase images were reconstructed using the standard vendor supplied reconstruction. In each breath hold, diffusion encoding was performed in 6 directions (identical to those described in the simulation section, applied in the magnet frame of reference) and also with small spoiler gradients in place of the diffusion encoding gradients (effective b_{ref}=34smm^{-2} with a constant direction of (1,1,1) in the (read, phase, slice) patient co-ordinate system). Crusher gradients were not used (see Lundell et al. (24) figure 1). cDTI acquisitions were performed at b_{main}=500,1000,1500 and 2000 smm^{-2} (b_{main} values, as elsewhere are prescribed values assuming RR interval=1000ms). The magnitude of the diffusion weighting was confirmed by exporting the gradient waveforms from the MRI simulator

and calculating the double integral described by Stejskal and Tanner (25). Cross-terms from the imaging gradients were found to contribute around 0.1% to the b-values used and were therefore neglected when calculating the tensor. 12 averages were used at each b_{main} and direction. To test the performance of complex averaging with an increased b_{ref}, an additional 2 averages (2 breath holds) were acquired with b=150smm^{-2} and 6 directions. The minimum TE was used for each acquisition, except for the b_{ref} acquisitions (b_{ref}=34smm^{-2} and b_{ref}=150smm^{-2}), which were acquired with the same TE as the corresponding b_{main} acquisition.

The diffusion tensor and the parameter maps were calculated for each b_{main} using the b_{ref}=34smm^{-2} data and then the b_{ref}=150smm^{-2} data with matching TE. The orientation of the diffusion weighting in the reference images was accounted for in the tensor calculation. As TE was the same for b_{ref} and b_{main} no correction for T2 decay was required. Processing was performed using a modified version of the software described previously(2,5,6). All images were visually assessed to exclude motion-corrupted frames before rigid registration. The processing code produced three versions of the diffusion tensor and parameter maps using the same image data for each b_{main}-b_{ref} pair (figure 1):

1. Magnitude processing – beat-to-beat heart rate correction.
   The processing was performed as in (2) taking the heart rate corrected b-value into account for every acquired image and including all of the magnitude images in the matrix inversion used to calculate the diffusion tensor without averaging.
2. Magnitude averaging – average heart rate correction.
   Magnitude data acquired with the same b-value and diffusion encoding direction was averaged and the b-value was corrected based on the average heart rate during acquisition of the data used.
3. Complex averaging – phase correction and average heart rate correction.
   The phase induced by residual bulk displacements between the diffusion encoding gradients causes signal cancellation after averaging. Therefore, the motion-induced phase of each image was approximated by the phase of a copy of the data multiplied in k-space with a pyramid shaped kernel of width ¼ of the FOV(16). This low-resolution phase was subtracted from the original images. All images with the same encoding direction and b-

value were averaged in the complex domain before calculating the magnitude. The b-value was corrected based on the average heart rate during acquisition of the data used.

In pixels where one or more eigenvalues were found to be negative (typically <0.5% of pixels in the left ventricle), the negative values were replaced with an average value from the surrounding pixels. SNR in the b_{ref}=34 smm^{-2} images was measured as in the simulations. The mean transmural helical angle gradient (HAg) was used to facilitate comparisons of HA. HAg was calculated from radial profiles using a linear regression of helical angle with transmural depth(2,12,26). The mean coefficient of determination (R^2) of this linear regression (HA-R^2) was used as a measure of the linearity of the transmural HA change. Mean left ventricular MD, FA, E2A, HAg, HA-R^2 and the eigenvalues were averaged over the left-ventricle, after excluding papillary muscle and the part of the septal wall considered right ventricular. Values were compared between the 4 b_{main} values and between the three methods. Where a histogram suggested normality, a repeated-measures ANOVA was used otherwise a Friedman test was used. Paired comparisons were performed using a t-test or a Wilcoxon test. In order to reduce the probability of type-I statistical errors, as many statistical comparisons were performed, a P-value threshold of 0.01 was used in all cases.

Results

Simulations

There was good agreement between the appearance of the parameters maps originating from both the noisy simulated data and *in-vivo* data from a normal subject acquired in a previous study (2) (figure 2).

The bias (simulated - input parameter) and absolute error (mean of the absolute simulated – input parameter) of the MD, FA, HA and E2A parameters is plotted against b_{main} for 3 simulated SNR values and each of the three reconstruction methods in figure 3 (b_{ref}=0, 12 averages). The corresponding plots for the three eigenvalues are shown in supplementary figure S1 and plots similar to figure 3 for all 9 SNR values are shown in supplementary figures S2, S3 and S4, for magnitude averaging, beat-to-beat correction and complex averaging respectively. At low b_{main}

MD and FA are over-estimated and E2A is under estimated using all 3 reconstruction methods. At high b_{main} using magnitude averaging and beat-to-beat correction MD, FA and E2A are under-estimated. There is a slight (<10°) over-estimation of HA at high and low b_{main} using all methods, but the primary effect of noise is to reduce the precision, as indicated by the increase in the absolute HA error.

Using magnitude averaging the value at which the effect of noise transitions from over- to under-estimation of FA is similar for all SNR values (b_{main}=1000 – 1250smm^{-2} for SNR<21 and b_{main}=750-1000smm^{-2} for SNR=21). The transition for MD generally occurs at a lower b_{main}; by b_{main}=250 smm^{-2} MD is under-estimated for all SNR<16 (SNR=21 transitions by b_{main}=1000smm^{-2}). The bias in E2A and the absolute error in all parameters shown in figure 3, is a minimum or very close to a minimum at b_{main}=1000smm^{-2}.

Using beat-to-beat correction reduces the magnitude of the bias in all parameters and reduces the absolute error in MD and FA when compared to magnitude averaging. This has the result of shifting the b-value corresponding to the minimum absolute error or bias to a higher b_{main}. By b_{main}=500smm^{-2} MD is under-estimated for the majority of SNR values studied and the transition from over to under-estimation of FA happens at 1250<b_{main}<1500smm^{-2}.

Using complex averaging, the under-estimation of FA at high b_{main} is eliminated at all SNR values studied and the under-estimation of MD is eliminated for all but the very highest (>2000smm^{-2}) b_{main} values.

The effect of increasing b_{ref} from 0 to 150smm^{-2} is shown in supplementary material figure S5. Increasing the reference b-value increases the magnitude of the bias in MD and E2A and increases the absolute error in all parameters at low b_{main} for all methods. A comparison of the number of averages used is provided in supplementary material figure S6. These results demonstrate a substantial reduction in errors when increasing from 4 to 8 averages, but minimal improvements when increasing the averages further to 12. The effects of the variation in RR-interval on the performance of each of the processing methods is shown in supplementary material figure S7. The performance of both complex and magnitude averaging shows little dependence on the variation in RR-interval. In contrast, when using beat-

to-beat correction the variation in RR-interval results in an increased error in MD. Supplementary material figures S8 and S9 show the effects of varying FA and MD, respectively. In general, a higher FA or MD value results in a lower optimal b_{main} value. There is an under-estimation of FA at low b-values when the ground truth FA is high (0.72). At all ground-truth FA values there is a small positive minimum FA bias for complex averaging that increases for decreasing ground-truth FA and at the lowest FA value (0.22) the bias for the complex averaged data increases with b_{main} at high b_{main}.

In-vivo imaging

cDTI parameter maps were calculated from data acquired in all subjects with all b_{main} values using all methods. The median of the mean RR-interval was 1.015s (range 0.798-1.27s) and histograms of the RR-intervals during the studies are shown in supplementary figure S10. At prescribed b_{main}=2000smm^{-2}, these RR intervals result in a median actual b_{main}=2029smm^{-2} (range 1596-2540smm^{-2}). Further statistical analysis (one-way repeated measures ANOVA with Greenhouse-Geisser correction for non-sphericity) was used to compare the RR-interval between diffusion encoding directions. This test found statistical differences between diffusion encoding directions in two subjects (both $P<10^{-3}$) and the subsequent paired testing demonstrated that this was a result of a difference in RR-interval between the b_{ref}=34smm^{-2} and the b_{main} images (RR increase of 4% for the b_{ref} images in one subject and a decrease of 4% in the other). The mean (±standard deviation) SNR in the unaveraged b_{ref}=34smm^{-2} images was 12.0±1.9. The median rate of rejection of acquired frames was 6% (range 0 – 35%) and there was no significant correlation with b-value (Pearson R=0.15, P=0.36). Background noise was visibly reduced in the complex averaged images when compared to the magnitude averaged images (figure 4).

Example parameter maps (MD, FA, HA and E2A) from one typical subject using b_{main}=2000smm^{-2} and b_{ref}=34smm^{-2} and all three methods are provided in figure 5. Additional parameters maps for all b_{main} and processing methods are provided in supplementary material figures S11-S14. As predicted by the simulations, figure 5 shows a visibly reduced MD when magnitude averaging is used. This MD reduction is partially compensated for by using complex averaging and, to a lesser by using

beat-to-beat correction. FA is increased in the mesocardial layer (see McGill et al. (27) for a discussion of this) and this effect is less evident in the magnitude-averaged images due to attenuation of the primary eigenvalue. There are several isolated pixels of high MD and FA (arrow heads) when using the beat-to-beat correction, which are absent using both of the averaging techniques. There are few visible changes in helical angle and E2A between the three methods.

Figure 6 compares the full tensor and the eigenvectors produced using all methods at b_{main}=2000smm^{-2} with b_{ref}=34smm^{-2} in one example. While the tensors are a similar shape and the eigenvectors are mostly similarly orientated, there are differences between the three methods, most clearly in the second eigenvector.

The MD, FA, E2A, HAg, HA-R^2 and each of the three eigenvalues are plotted as the mean ± standard deviation across the 10 subjects with b_{main} in figure 7 (also see figure S15, b_{ref}=150smm^{-2}). All parameters except HA-R^2 were deemed to be normally distributed. There is a significant reduction in MD with b_{main} (using all methods) which is partly compensated when using complex averaging or beat-to-beat correction. FA also reduces with b_{main} using magnitude averaging, but not using complex averaging. At b_{main}=2000smm^{-2} there is a significant difference when comparing magnitude vs. complex and magnitude vs. beat-to-beat corrected data for both MD and FA. By this maximum b_{main} value, there is a 13% difference in FA and a 7% difference in MD between the complex and magnitude averaged data.

There were no significant differences in E2A values between b_{main} values or averaging methods.

Each of the eigenvalues reduces with increasing b_{main} independent of the averaging method used. The reduction in the 1st eigenvalue is partially compensated when using complex averaging and, to a lesser extent using beat-to-beat correction. At b_{main}=2000smm^{-2} this results in a significantly higher 1st eigenvalue using complex averaging than using magnitude averaging or beat-to-beat correction. At b_{main}=500 smm^{-2}, significant differences in MD and the 1st eigenvalue are present between complex and magnitude averaged data and in the second eigenvalue between the magnitude averaged and both the complex averaged and the beat-to-beat corrected data. The magnitude of these differences, is however, small. There were no

significant differences in HAg between b_{main} values or methods, except at b_{main}=1500smm^{-2}, where HAg using magnitude averaging is larger than when using beat-to-beat correction. The median value of HA-R^2 was greatest at b_{main}=1500smm^{-2}, but there were no significant differences between b_{main} values or methods.

There are similar trends when b_{ref}=150 smm^{-2} is used (figure S15). In this case there were significant differences at b_{main}=2000smm^{-2} between FA values calculated using magnitude and complex averaging. Also at b_{main}=2000smm^{-2} there were significant differences in the 1st eigenvalues calculated using magnitude averaging and either of the complex averaging or beat-to-beat correction. There were significant differences in HAg between methods at b_{main}=1500smm^{-2}, and HA-R^2 at b_{main}=2000smm^{-2}, but post-hoc tests found no significant results. There was also a significant difference in HA-R^2 between b_{main} values using beat-to-beat correction.

Discussion

Using simulations we have shown the effects of noise on the parameters typically derived from the diffusion tensor in cDTI. At low b_{main}, the eigenvalue repulsion described in early DTI studies(10) results in over-estimation of FA. In this regime, eigenvalue repulsion can cause the 3rd eigenvalue to be negative, which is unphysical so our processing algorithm replaces these values with the average from neighbouring pixels. This causes an over-estimation of MD at low b_{main}. At high b_{main}, the noise floor results in a reduced MD and FA, described by Jones and Basser (11) as “squashing the peanut”. The main effect of noise on the HA was a loss of precision which is reflected in the increase in standard deviation and absolute error. E2A is under-estimated at high and low b_{main}. In general an increase in image noise leads to a loss of both precision and accuracy. This is reflected in a noisier parameter map and a larger magnitude in the bias. The optimum b_{main} depends on the expected MD and FA of the tissue and to some extent SNR. The b_{main} corresponding to zero bias appears to be relatively independent of the noise, at b_{main}=1000-1250smm^{-2} (although it may be higher when FA is low). The bias in MD crosses or approaches zero by b_{main}=250smm^{-2} (assuming the typical diffusion parameters measured in previous studies using similar techniques). As previous *in-vivo* cDTI studies (1,3,17) have typically used b_{main}=200-600smm^{-2}, our results suggest that FA was probably over-estimated, while MD and E2A were likely under-estimated.

Using cDTI specific simulations we demonstrated that in the high b_{main} regime the under-estimation of MD (b_{main}>250smm^{-2} – 1000smm^{-2} depending on SNR) and FA (b_{main}≥1250smm^{-2}) observed with magnitude averaging can be compensated for by averaging the complex data. This is a consequence of reducing the noise floor, which avoids the attenuation of the 1st and, at very high b_{main}, the 2nd eigenvalue. At low and intermediate FA values (0.22 and 0.42), eigenvalue repulsion causes an over-estimation of FA at low b_{main}. Whereas at low b_{main} and high FA values, where the 3rd eigenvalue is very small, the replacement of eigenvalues which have been driven negative by eigenvalue repulsion with neighbouring positive values results in an under-estimation of FA. These effects cannot be compensated for by using complex averaging.

The absolute error in all parameters is a lowest for almost all simulations when using complex averaging except when there is a low ground-truth FA (0.22) and high b_{main} (>1250smm^{-2}). In this regime eigenvalue repulsion causes an increase in the FA bias, before the noise floor effects cause a reduction in FA (also shown in Jones and Basser (11)).

In vivo we observed the reduction of MD and FA with increasing b_{main} predicted by the simulations when using magnitude averaging. By approximating the motion-induced phase in the diffusion-weighted images by a low-resolution copy of the image phase, we were able to demonstrate reduced background signal intensity. Averaging the complex data resulted in a smaller reduction in MD with increasing b_{main} than when averaging the magnitude data. Complex averaging also eliminated the reduction in FA associated with increasing b_{main}. Analysis of the eigenvalues demonstrated that the recovery of the lost MD and FA at high b_{main} by complex averaging is primarily achieved by recovering losses in the first eigenvalue. In agreement with the simulations, there were no differences in E2A between any of the methods *in vivo* and the E2A plotted with b_{main} is concave for both *in-vivo* and simulation data. The linear variation of HA with transmural depth makes it difficult to directly compare helical angles, but there were few differences in HAg between methods and none between b_{main} values. Although the peak in HA-R^2 (P=non-significant) suggests that HA might be most linear around b_{main}=1500smm^{-2}. When

we compared tensors produced by the three methods (figure 6) there were visual differences.

One potential limitation of complex averaging is that beat-to-beat correction of the b-value for heart rate cannot be performed. However, our simulations suggest that as long as the mean RR-interval is used with complex or magnitude averaging, typical variations in heart rate do not result in an increase in error. We did not include variations in RR-interval between diffusion encoding directions in our simulations and analysis of our *in-vivo* data suggests that in a minority of subjects (2/10) there is a significant change in heart rate during the breath hold. As these changes were only found between the b_{ref}=34smm^{-2} images (acquired before the b_{main} images in each breath hold) and the b_{main} images and not between the b_{main} images, the effect on the derived parameters is mainly restricted to a small change in MD for the complex and magnitude averaged data (+0.6% in one subject and -2% in the other). Future studies should avoid these effects by, for example: varying the order in which data is acquired between breath holds (including reference data); using the RR-interval calculated by diffusion direction; or acquiring data for a single diffusion encoding direction in each breath hold.

In agreement with the simulations, beat-to-beat correction generally performs better than magnitude averaging, but not due to the obvious ability to correct for beat-to-beat variations in the RR-interval. The inclusion of the unaveraged images in the matrix inversion used to calculate the diffusion tensor avoids the magnitude averaging step and therefore, reduces the noise floor effects. As b_{main} increases the MD, FA and 1st eigenvalue are less severely attenuated when using beat-to-beat correction than when using magnitude averaged data, but complex averaging performs better still. At the highest b_{main} values, the FA and MD reconstructed with beat-to-beat correction contained several pixels which appeared to be spurious and not consistent with the surrounding pixels or with the other methods (figure 5). These pixels corresponded to pixels where one average had a very low signal intensity. This has minimal effect when the data is averaged before calculating the natural logarithm required before the matrix inversion, but skews the calculated diffusion when the logarithm of each of the signal intensities is calculated and included in the linear least squares inversion. In future studies, this effect could be avoided using a pre-processing step. The simulations also show that when using complex averaging

there is an increase in the minimum FA bias with decreasing ground-truth FA, although this effect is also present with magnitude averaging and beat-to-beat correction. A further limitation is that complex averaging was unable to fully compensate for reductions in MD with increasing b_{main}. There is a significant reduction in all eigenvalues with increasing b_{main}. While the simulations suggest that this might be the result of noise, it may also represent non-Gaussian diffusion at high b-values(28).

A further issue in cDTI is the effect of motion, which we have not directly addressed in this work. The amount of motion-induced phase in the DTI data will increase with b-value. Eventually this will lead to signal loss, due to a sufficient range of phases present within each voxel. This effect would be independent of the averaging technique used. In this work we assumed that the motion induced phase varied gradually across the image, but this assumption could be violated at sufficiently high b-values or with sufficient motion. While this would affect the performance of complex averaging, in this work we were able to perform complex averaging with data acquired using $b \leq 2000 s mm^{-2}$ and did not observe artefacts consistent with violation of this assumption. Previous work (29,30) has simulated the effects of motion in spin-echo based cDTI techniques, but there is a need to extend this work to STEAM which we hope to address in future.

In order to most realistically compare sequence parameters as they would be used in future studies, we used the minimum TE for each b_{main}. This means that the effect of changing b_{main} is intertwined with that of changing TE. In contrast, if TE was maintained, the b_{main} corresponding to the minimum parameter error is artificially inflated. This also means that our results are specific to STEAM cDTI sequences. For spin-echo based sequences we may expect a higher SNR despite the much longer TE required, but we would expect the curves to have a similar shape to those shown here.

We did not account for variations in SNR with heart rate in our simulations. While there is a loss of SNR with decreasing heart rate due to T1 recovery during the longer mixing time in the STEAM sequence, there is also an increase in SNR due to the increased T1 recovery time between stimulated echoes. As a result, the SNR dependence on heart rate is relatively small for this sequence.

In previous work(2) we found a combination of b_{main}=750smm^{-2} and b_{ref}=150smm^{-2} to be optimal from a range tested, but we did not have a reference value for FA. The simulations performed here suggest that for minimum error in FA, b_{main}=1000-1250smm^{-2} is preferable. While there is some dependence on the SNR, the minimum absolute error in MD, HA and E2A also lies close to b_{main}=1000smm^{-2} and this would, therefore seem like a good choice in future studies. If complex averaging can be performed then a higher b_{main} can be used. With prescribed b_{main}=1250smm^{-2} any under-estimation of MD and FA can be compensated for with complex averaging. The use of a sufficiently high b_{main} avoids the uncorrectable over-estimation of FA at low b_{main} values, even in the presence of a raised heart rate of 75 beats per minute, where a prescribed b_{main}=1250smm^{-2} gives an actual value of 1000smm^{-2}. Several previous studies have investigated the optimal b-values with regards to brain DTI studies (31,32,33). Despite the different sequences and T2 values studies were based on, the optimal b_{main} of 900smm^{-2} typically suggested for brain DTI is relatively similar to the optimal values found here. Jones and Basser (11) provided an order of magnitude estimate for the maximum b_{main} that could be used without sampling the noise floor. For FA=0.42, MD=0.9x10^{-3}mm^{2}s^{-1} and SNR=11 the maximum b_{main} is predicted as 1600smm^{-2}. While this is higher than our optimal b_{main}, at this value our simulations predict an under-estimation in FA of only 0.03.

The MD values measured here are larger than those we found in previous work using a similar sequence and beat-to-beat correction(2). Using b_{ref}=34smm^{-2} and b_{main}=500smm^{-2} in this work we found MD=1.071±0.062mm^{2}s^{-1} compared to MD=0.983±0.041mm^{2}s^{-1} using b_{ref}=15smm^{-2} and b_{main}=550smm^{-2}. These changes are likely the result of using 12 averages in this work and a SENSE rather than GRAPPA reconstruction. The SNR is similar between the two reconstructions (12.0±1.9 SENSE, vs. 12.1±1.55 GRAPPA, P=0.9), but the noise floor was higher in the GRAPPA images. The standard manufacturer provided reconstructions were used in this work without optimisation. However, there are known differences in the noise floor distribution between the sum of squares reconstruction used with GRAPPA and the coil sensitivity weighted combination used with SENSE(34,35).

FA was similar when using b_{main}=500/550smm^{-2}, b_{ref}=34/15smm^{-2} at 0.409±0.027 compared with 0.411±0.026 in previous work, but higher in this study using

b_{main}=1000/950smm^{-2} at 0.410±0.042 compared with 0.372±0.029 in the previous work. This loss of FA and MD at b_{main}=950smm^{-2} in the previous work is consistent with noise floor effects which are shifted to higher b_{main} in this work by using the SENSE reconstruction. The healthy systolic E2A in previous work (6) had a median of 56.4° (b_{main}=350, b_{ref}=135smm^{-2}, similar sequence) which is similar to our value of 55±10° (median ± interquartile range).

Previous simulations have been created to study the effects of cardiac motion on diffusion-weighted imaging(29,36) and the effects of resolution and SNR on the measured cardiomyocyte orientation(37). This is the first cDTI specific simulation to consider the effects of noise on the DTI parameters of interest in the heart using realistic parameters. In this work we did not consider the effects of the number of diffusion encoding directions, which may affect the behaviour of cDTI parameters in the presence of noise. However, in future, these simulations could be adapted to study these effects and other acquisition or reconstruction parameters including alternative noise reduction algorithms and non-Gaussian models of diffusion.

A wealth of techniques have been employed for noise reduction in MRI(38) and many of them are applicable to diffusion tensor imaging(11,39). However, most require SNR estimates or noise distributions, involve complex reconstructions, add smoothing or remove small/low contrast objects. While complex averaging has found limited applicability in neurological DTI(40), the averaging used in cDTI makes it a more suitable target. Complex averaging does not affect spatial resolution and, as long as the motion induced phase can be identified, it will not introduce artefacts. Complex averaging is not limited to STEAM-EPI data and could be applied to diffusion weighted imaging and spin-echo cDTI. While we did not investigate more advanced methods of calculating the diffusion tensor, including weighted least-squares and non-linear methods, which may reduce the effects of noise, complex averaging should be able to be readily combined with such techniques in future. Estimating the image phase is also an important step towards a segmented acquisition for improved spatial resolution(41).

In conclusion, the effect of noise on parameters derived from cDTI depends on the parameters themselves, the SNR, the averaging method used in calculating the diffusion tensor and the magnitude of the diffusion weighting. The optimal b_{main}

depends on the SNR to a small extent and the actual FA and MD of the tissue being studied. For the most accurate measurements, a b_{main} of 1000 - 1250 smm^{-2} should be used. The high b_{main} regime is preferable over the low, as the under-estimation of FA and MD can be compensated for by using complex averaging with a relatively straightforward correction for motion induced image phase. The ability to perform cDTI at high b_{main} may also enable new insights into myocardial microstructure.

Acknowledgement

The work was supported by the National Institute for Health Research Cardiovascular Biomedical Research Unit of Royal Brompton and Harefield NHS Trust and Imperial College. London UK

References

1. Nielles-Vallespin S, Mekkaoui C, Gatehouse P, Reese TG, Keegan J, Ferreira PF, Collins S, Speier P, Feiweier T, de Silva R, Jackowski MP, Pennell DJ, Sosnovik DE, Firmin D. In vivo diffusion tensor MRI of the human heart: reproducibility of breath-hold and navigator-based approaches. Magn Reson Med 2013; 70: 454-65.
2. Scott AD, Ferreira PFADC, Nielles-Vallespin S, Gatehouse P, McGill L, Kilner P, Pennell DJ, Firmin DN. Optimal diffusion weighting for in vivo cardiac diffusion tensor imaging. Magn Reson Med 2014; 74: 420-30.
3. Stoeck CT, von Deuster C, Genet M, Atkinson D, Kozerke S. Second-Order Motion-Compensated Spin Echo Diffusion Tensor Imaging of the Human Heart. Magnetic Resonance in Medicine 2015; doi: 10.1002/mrm.25784. [Epub ahead of print].
4. Lau AZ, Tunnicliffe EM, Frost R, Koopmans PJ, Tyler DJ, Robson MD. Accelerated human cardiac diffusion tensor imaging using simultaneous multislice imaging. Magn Reson Med 2014; 73: 995-1005.
5. McGill L, Ismail TF, Nielles-Vallespin S, Ferreira P, Scott AD, Roughton M, Kilner PJ, Ho SY, McCarthy KP, Gatehouse PD, de Silva R, Speier P, Feiweier T, Mekkaoui C, Sosnovik DE, Prasad SK, Firmin DN, Pennell DJ. Reproducibility of in-vivo diffusion tensor cardiovascular magnetic resonance in hypertrophic cardiomyopathy. J Cardiovasc Magn Reson 2012; 14: 86.
6. Ferreira PF, Kilner PJ, McGill L, Nielles-Vallespin S, Scott AD, Ho SY, McCarthy KP, Haba MM, Ismail TF, Gatehouse PD, de Silva R, Lyon AR, Prasad SK, Firmin DN, Pennell DJ. In vivo cardiovascular magnetic resonance diffusion tensor imaging shows evidence of abnormal myocardial laminar orientations and mobility in hypertrophic cardiomyopathy. J Cardiovasc Magn Reson 2014; 16: 87.
7. Kim S, Chi-Fishman G, Barnett AS, Pierpaoli C. Dependence on diffusion time of apparent diffusion tensor of ex vivo calf tongue and heart. Magn Reson Med 2005; 54: 1387-96.
8. Reese, Wedeen, Weisskoff. Measuring Diffusion in the Presence of Material Strain. J Magn Reson B 1996; 112: 253-8.
9. Stoeck CT, Kalinowska A, von Deuster C, Harmer J, Chan RW, Niemann M, Manka R, Atkinson D, Sosnovik DE, Mekkaoui C, Kozerke S. Dual-phase cardiac diffusion tensor imaging with strain correction. PLoS One 2014; 9: e107159.

10. Bastin ME, Armitage PA, Marshall I. A theoretical study of the effect of experimental noise on the measurement of anisotropy in diffusion imaging. Magn Reson Imaging 1998; 16: 773-85.
11. Jones DK, Basser PJ. "Squashing peanuts and smashing pumpkins": how noise distorts diffusion-weighted MR data. Magn Reson Med 2004; 52: 979-93.
12. Tunnicliffe EM, Scott AD, Ferreira P, Ariga R, McGill L, Nielles-Vallespin S, Neubauer S, Pennell DJ, Robson MD, Firmin DN. Intercentre reproducibility of cardiac apparent diffusion coefficient and fractional anisotropy in healthy volunteers. J Cardiovasc Magn Reson 2014; 16: 31.
13. Streeter DD Jr, Spotnitz HM, Patel DP, Ross J Jr, Sonnenblick EH. Fiber orientation in the canine left ventricle during diastole and systole. Circ Res 1969; 24: 339-47.
14. Spotnitz HM, Spotnitz WD, Cottrell TS, Spiro D, Sonnenblick EH. Cellular basis for volume related wall thickness changes in the rat left ventricle. J Mol Cell Cardiol 1974; 6: 317-31.
15. Hales PW, Schneider JE, Burton RAB, Wright BJ, Bollensdorff C, Kohl P. Histo-anatomical structure of the living isolated rat heart in two contraction states assessed by diffusion tensor MRI. Prog Biophys Mol Biol 2012; 110: 319-30.
16. Pipe JG, Farthing VG, Forbes KP. Multishot diffusion-weighted FSE using PROPELLER MRI. Magn Reson Med 2002; 47: 42-52.
17. Reese TG, Weisskoff RM, Smith RN, Rosen BR, Dinsmore RE, Wedeen VJ. Imaging myocardial fiber architecture in vivo with magnetic resonance. Magn Reson Med 1995; 34: 786-91.
18. Ennis DB, Kindlmann G. Orthogonal tensor invariants and the analysis of diffusion tensor magnetic resonance images. Magn Reson Med 2006; 55: 136-46.
19. Dou J, Reese TG, Tseng WI, Wedeen VJ. Cardiac diffusion MRI without motion effects. Magn Reson Med 2002; 48: 105-14.
20. Nguyen C, Fan Z, Xie Y, Dawkins J, Tseliou E, Bi X, Sharif B, Dharmakumar R, Marbán E, Li D. In vivo contrast free chronic myocardial infarction characterization using diffusion-weighted cardiovascular magnetic resonance. J Cardiovasc Magn Reson 2014; 16: 68.
21. von Deuster C, Stoeck CT, Genet M, Atkinson D, Kozerke S. Spin echo versus stimulated echo diffusion tensor imaging of the in vivo human heart. Magn Reson Med 2015; doi: 10.1002/mrm.25998. [Epub ahead of print].

22. Wu M, Tseng WI, Su MM, Liu C, Chiou K, Wedeen VJ, Reese TG, Yang C. Diffusion tensor magnetic resonance imaging mapping the fiber architecture remodeling in human myocardium after infarction: correlation with viability and wall motion. Circulation 2006; 114: 1036-45.
23. Tseng WI, Dou J, Reese TG, Wedeen VJ. Imaging myocardial fiber disarray and intramural strain hypokinesis in hypertrophic cardiomyopathy with MRI. J Magn Reson Imaging 2006; 23: 1-8.
24. Lundell H, Alexander DC, Dyrby TB. High angular resolution diffusion imaging with stimulated echoes: compensation and correction in experiment design and analysis. NMR Biomed 2014; 27: 918-25.
25. Stejskal E, Tanner J. Spin diffusion measurements: Spin echoes in the presence of a time-dependent field gradient. The journal of chemical physics 1965; 42: 288--292.
26. Lombaert H, Peyrat J, Croisille P, Rapacchi S, Fanton L, Cheriet F, Clarysse P, Magnin I, Delingette H, Ayache N. Human atlas of the cardiac fiber architecture: study on a healthy population. IEEE Trans Med Imaging 2012; 31: 1436-47.
27. McGill L, Scott AD, Ferreira PF, Nielles-Vallespin S, Ismail T, Kilner PJ, Gatehouse PD, de Silva R, Prasad SK, Giannakidis A, Firmin DN, Pennell DJ. Heterogeneity of Fractional Anisotropy and Mean Diffusivity Measurements by In Vivo Diffusion Tensor Imaging in Normal Human Hearts. PLoS One 2015; 10: e0132360.
28. Hsu EW, Buckley DL, Bui JD, Blackband SJ, Forder JR. Two-component diffusion tensor MRI of isolated perfused hearts. Magn Reson Med 2001; 45: 1039-45.
29. Gamper U, Boesiger P, Kozerke S. Diffusion imaging of the in vivo heart using spin echoes--considerations on bulk motion sensitivity. Magn Reson Med 2007; 57: 331-7.
30. Welsh CL, DiBella EVR, Hsu EW. Higher-Order Motion-Compensation for In Vivo Cardiac Diffusion Tensor Imaging in Rats. IEEE Trans Med Imaging 2015; 34: 1843-53.
31. Armitage PA, Bastin ME. Utilizing the diffusion-to-noise ratio to optimize magnetic resonance diffusion tensor acquisition strategies for improving measurements of diffusion anisotropy. Magn Reson Med 2001; 45: 1056-65.
32. Jones DK, Horsfield MA, Simmons A. Optimal strategies for measuring

diffusion in anisotropic systems by magnetic resonance imaging. Magn Reson Med 1999; 42: 515-25.
33. Taylor PA, Biswal B. Geometric analysis of the b-dependent effects of Rician signal noise on diffusion tensor imaging estimates and determining an optimal b value. Magn Reson Imaging 2011; 29: 777-88.
34. Dietrich O, Heiland S, Sartor K. Noise correction for the exact determination of apparent diffusion coefficients at low SNR. Magn Reson Med 2001; 45: 448-53.
35. Sotiropoulos SN, Moeller S, Jbabdi S, Xu J, Andersson JL, Auerbach EJ, Yacoub E, Feinberg D, Setsompop K, Wald LL, Behrens TEJ, Ugurbil K, Lenglet C. Effects of image reconstruction on fiber orientation mapping from multichannel diffusion MRI: reducing the noise floor using SENSE. Magn Reson Med 2013; 70: 1682-9.
36. Wei H, Viallon M, Delattre BMA, Wang L, Pai VM, Wen H, Xue H, Guetter C, Croisille P, Zhu Y. Assessment of cardiac motion effects on the fiber architecture of the human heart in vivo. IEEE Trans Med Imaging 2013; 32: 1928-38.
37. Wang L, Zhu Y, Li H, Liu W, Magnin IE. Multiscale modeling and simulation of the cardiac fiber architecture for DMRI. IEEE Trans Biomed Eng 2012; 59: 16-9.
38. Mohan J, Krishnaveni V, Guo Y. A survey on the magnetic resonance image denoising methods. Biomedical Signal Processing and Control 2014; 9: 56--69.
39. Frindel C, Robini M, Croisille P, Zhu Y. Comparison of regularization methods for human cardiac diffusion tensor MRI. Med Image Anal 2009; 13: 405-18.
40. Bammer R, Holdsworth SJ, Veldhuis WB, Skare ST. New methods in diffusion-weighted and diffusion tensor imaging. Magn Reson Imaging Clin N Am 2009; 17: 175-204.
41. Jensen JH, Helpern JA, Ramani A, Lu H, Kaczynski K. Diffusional kurtosis imaging: The quantification of non-gaussian water diffusion by means of magnetic resonance imaging. Magn Reson Med 2005; 53: 1432-1440.

Figures

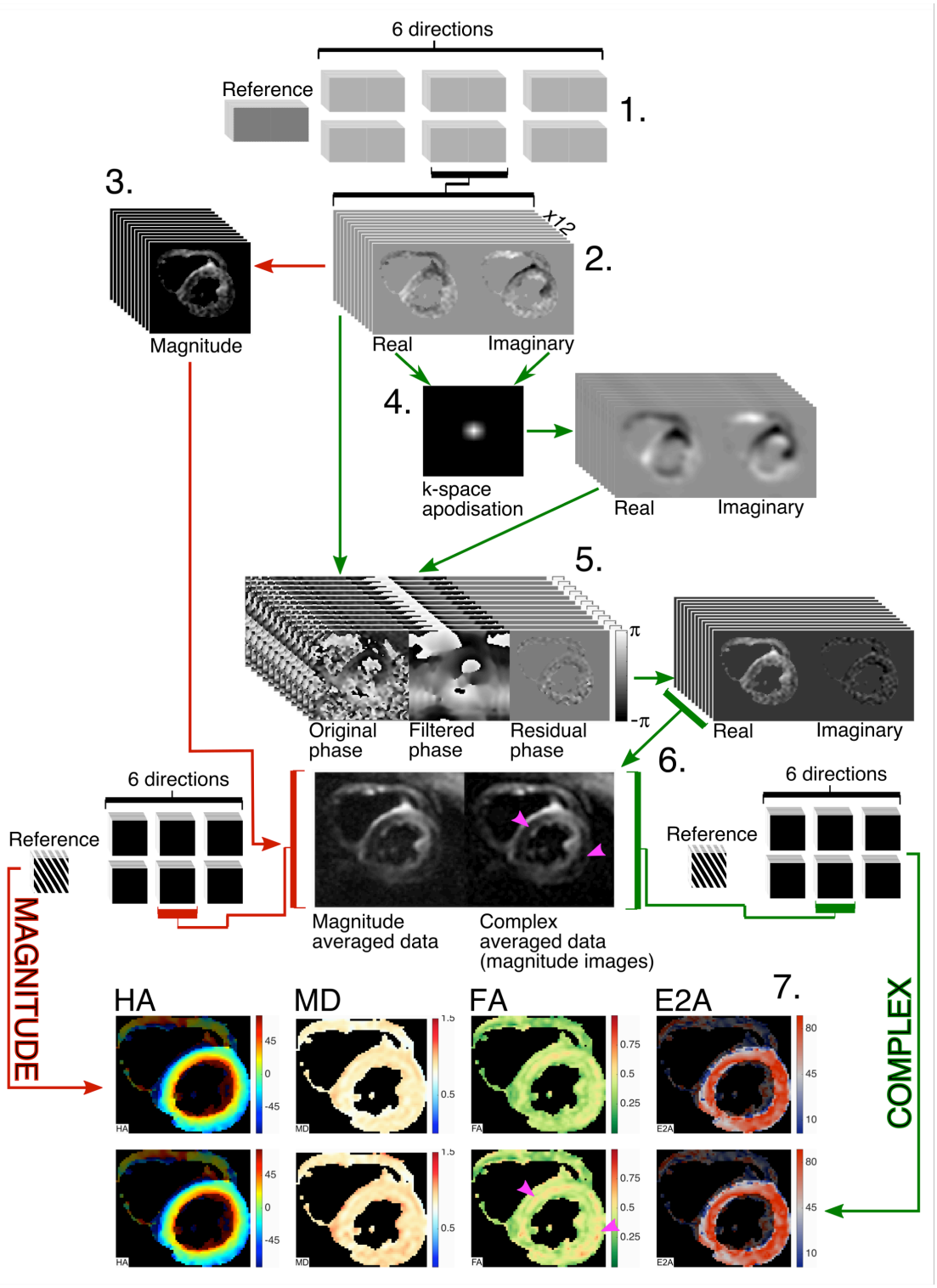

Figure 1: A comparison of the magnitude and complex averaging algorithms used for *in vivo* data. This example uses b_{main}=2000smm^{-2} and b_{ref}=34smm^{-2}.

1. For each b_{main} 12 averages of each encoding direction, 12 averages of b_{ref}=34smm^{-2} (with a constant direction) and 2 averages of each 6 directions for

b_{ref}=150smm^{-2} are acquired (b_{ref}=150smm^{-2} not shown).

2. Real and imaginary data for each direction and average.

3. For magnitude averaging, the magnitude image is calculated and the 12 images are averaged.

4. For complex averaging the real and imaginary images are multiplied by a pyramid shaped window (width ¼ FOV) in k-space to provide low-resolution copies(16).

5. The phase of the low-resolution images (filtered phase) contains the phase induced by differences in the heart's position between encoding and unencoding gradients. This is subtracted from the original phase which is combined with the original magnitude data.

6. Repeat steps 4 and 5 for every image. Real and imaginary images are averaged before calculating the magnitude. There is now one magnitude averaged and one complex averaged image for each encoding direction and b-value. The complex averaged data show reduced background noise levels (magenta arrow heads).

7. Parameter maps are calculated from the magnitude and complex averaged data. There are areas of higher FA (arrow heads) in the complex averaged data.

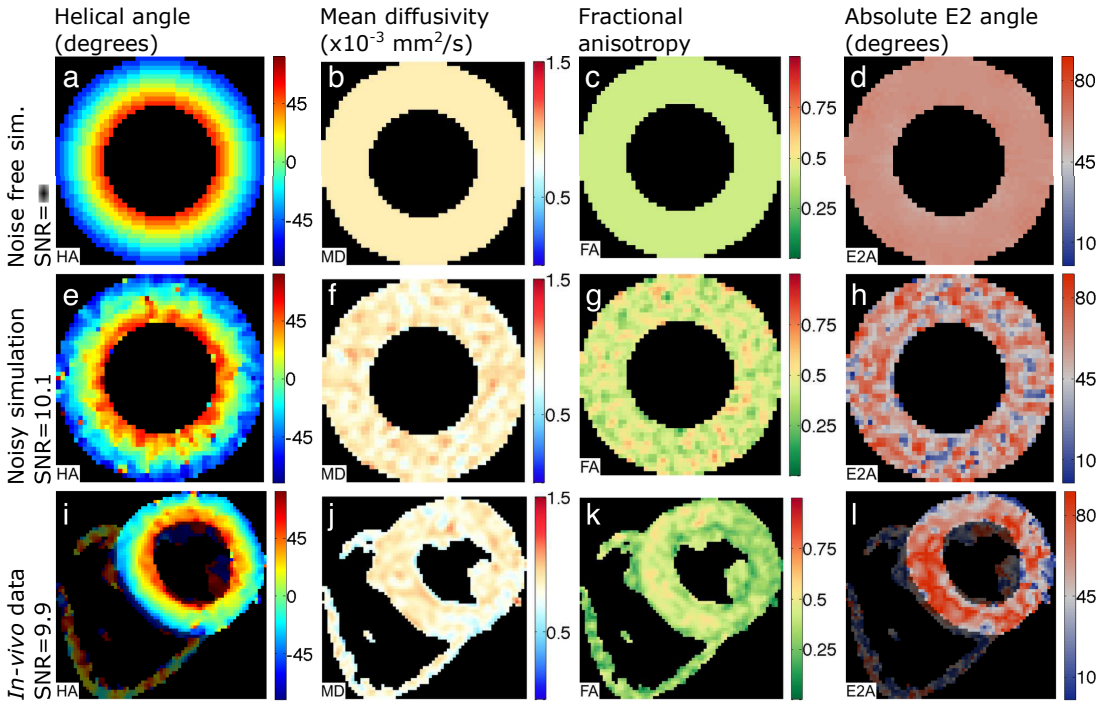

Figure 2: Simulated cDTI parameter maps without noise (top row), with added noise (b_{main}=800 smm^{-2}, 7 averages, middle row) and *in vivo* data with a similar SNR (b_{main}=750 smm^{-2}, 8 averages, bottom row).

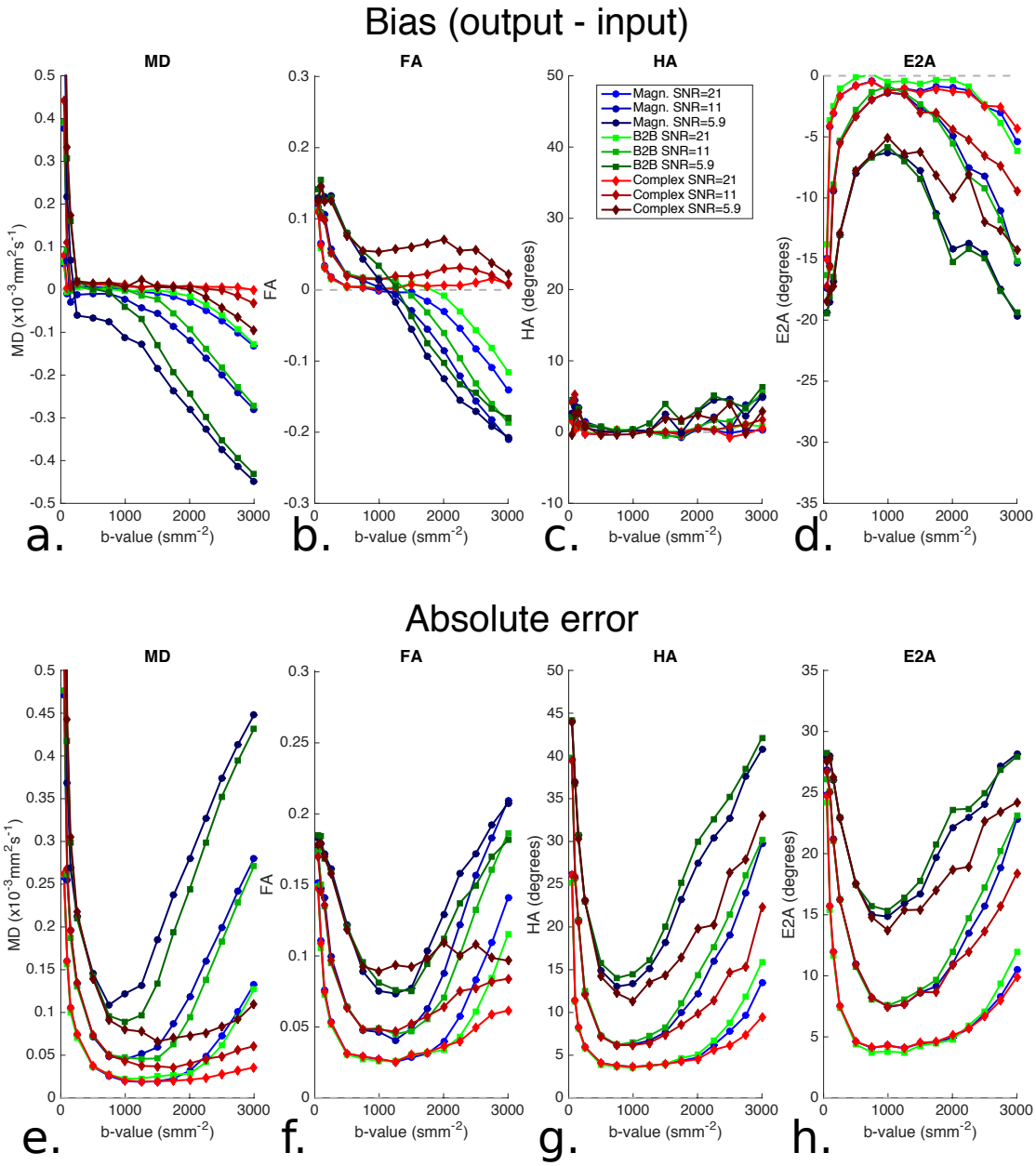

Figure 3: The mean bias (output parameter – ground truth) and absolute error in MD, FA, HA and E2A plotted with the b_{main} for the simulations using magnitude averaging, beat-to-beat correction and complex averaging. Simulations used 12 averages and SNR=11 in the b_{ref}=0 images with sufficient TE to achieve b_{main}=750smm^{-2}.

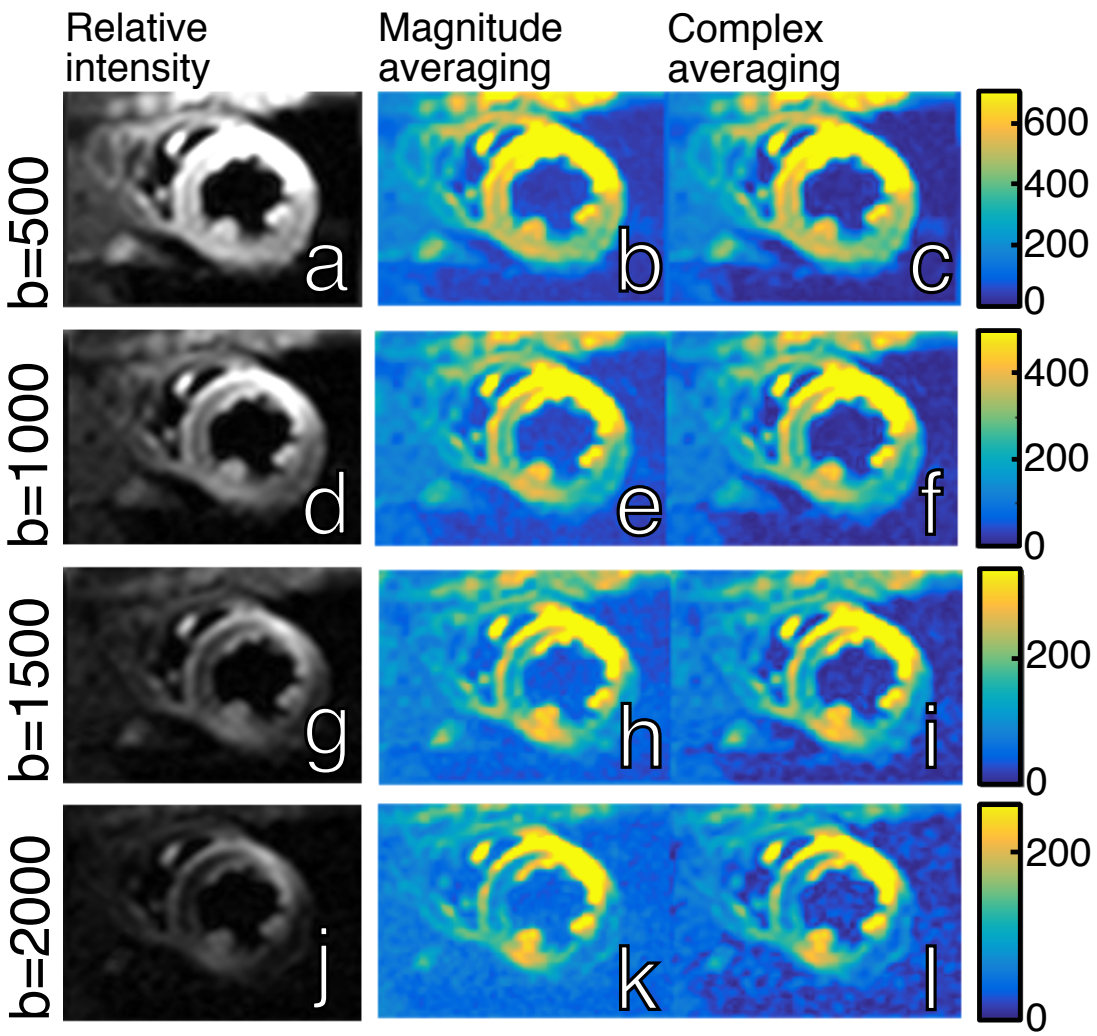

Figure 4: Example *in-vivo* images with diffusion encoding in one direction for all b-values (in smm^{-2}). The magnitude images are shown in grayscale with a constant window and level (first column). The magnitude and complex averaged images are shown using a colour map to highlight differences in the relative noise levels.

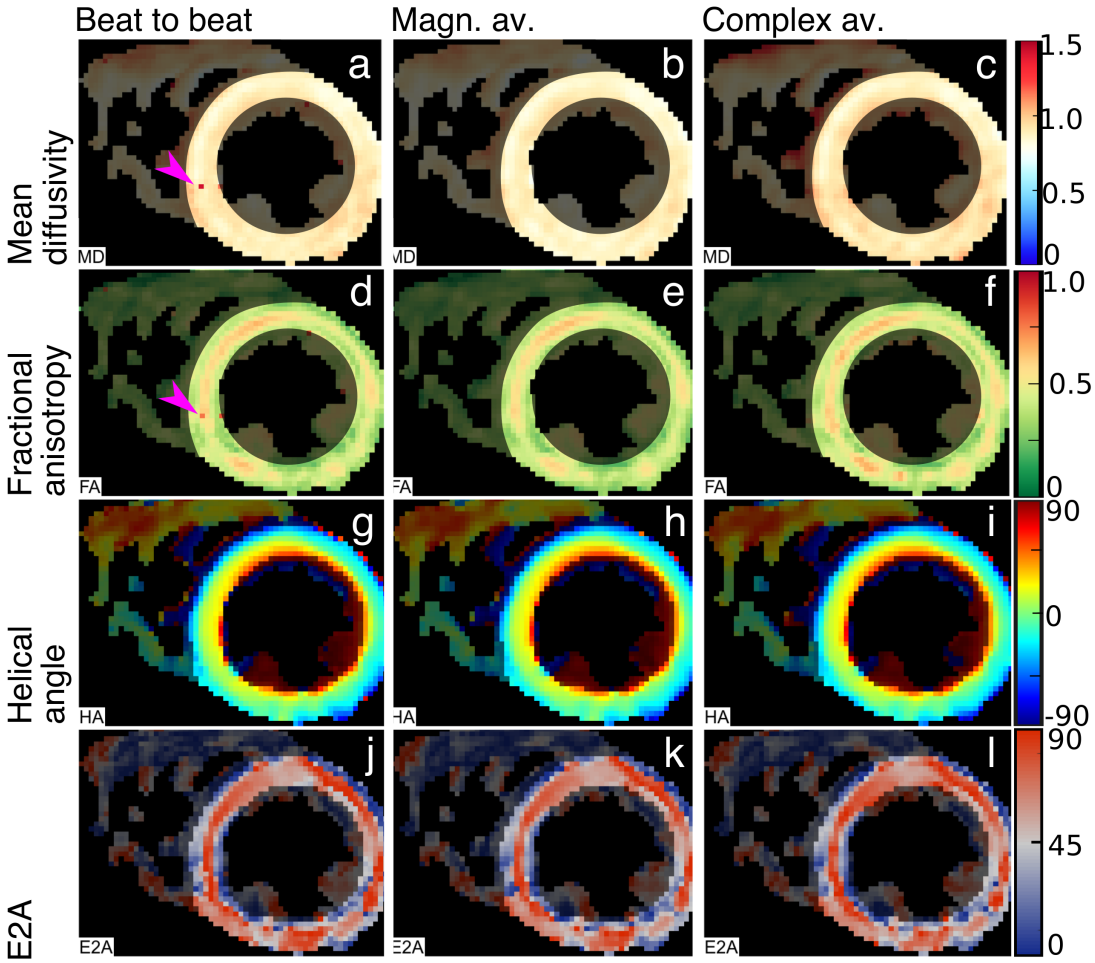

Figure 5: Example maps of mean diffusivity (MD), fractional anisotropy (FA), helical angle and E2A calculated using all three methods from data acquired at b_{main}=2000smm^{-2}. MD is visibly increased and the band of elevated FA is more prominent when using complex rather than magnitude averaging (see McGill et al. (27) for a discussion of this band). Several pixels in the MD and FA map have values inconsistent with the surroundings when the beat-to-beat method is used (arrow head indicates one). The shaded area in each image indicates the region of the image removed for quantitative comparison of the parameters.

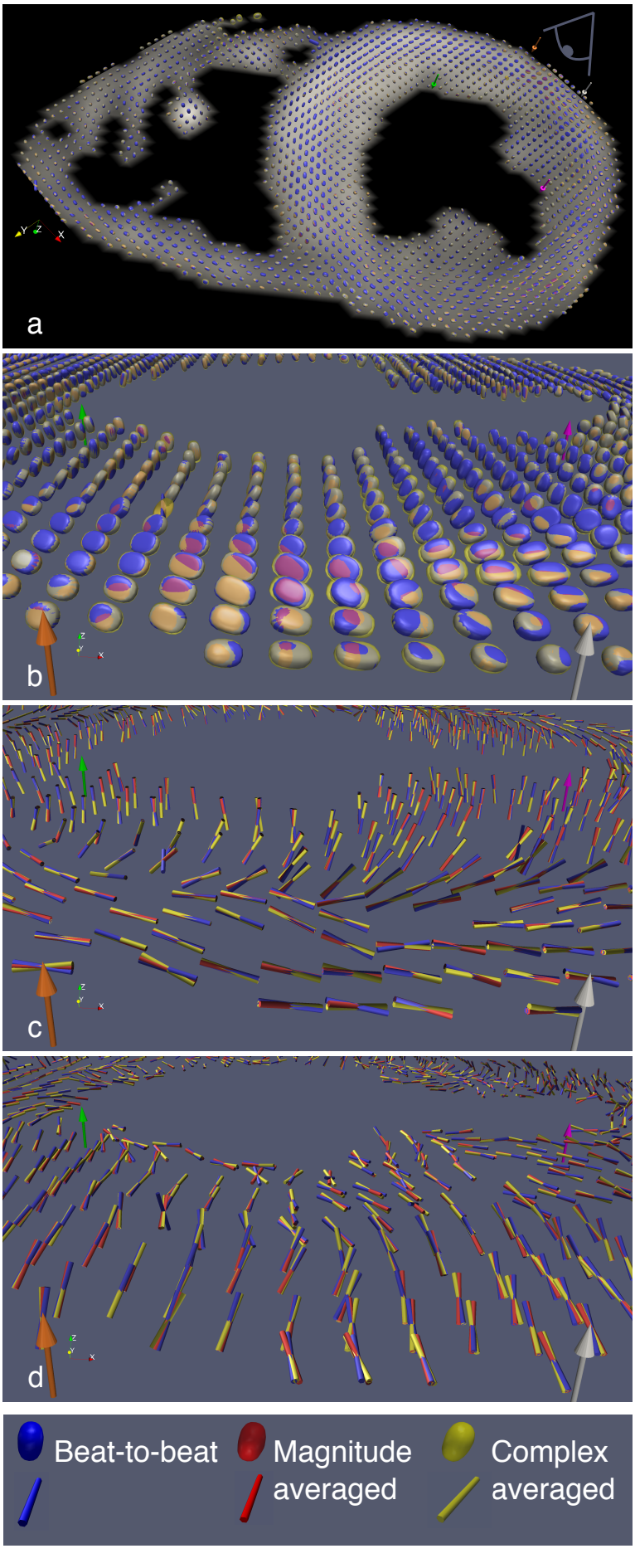
a
b
c
d
Beat-to-beat
Magnitude averaged
Complex averaged

Figure 6: A comparison of the diffusion tensors calculated by the three methods in an example subject at b_{main}=2000smm^{-2}. Superquadric glyphs representing the full diffusion tensor are shown in a and b (zoomed). Each method is shown by a semi-transparent glyph at each pixel (3 overlaid gyphs per pixel). The orientation of the primary and secondary eigenvectors are shown in b and c respectively. The orientation and size of the zoomed region is shown on a by the eye symbol and the arrows in all parts.

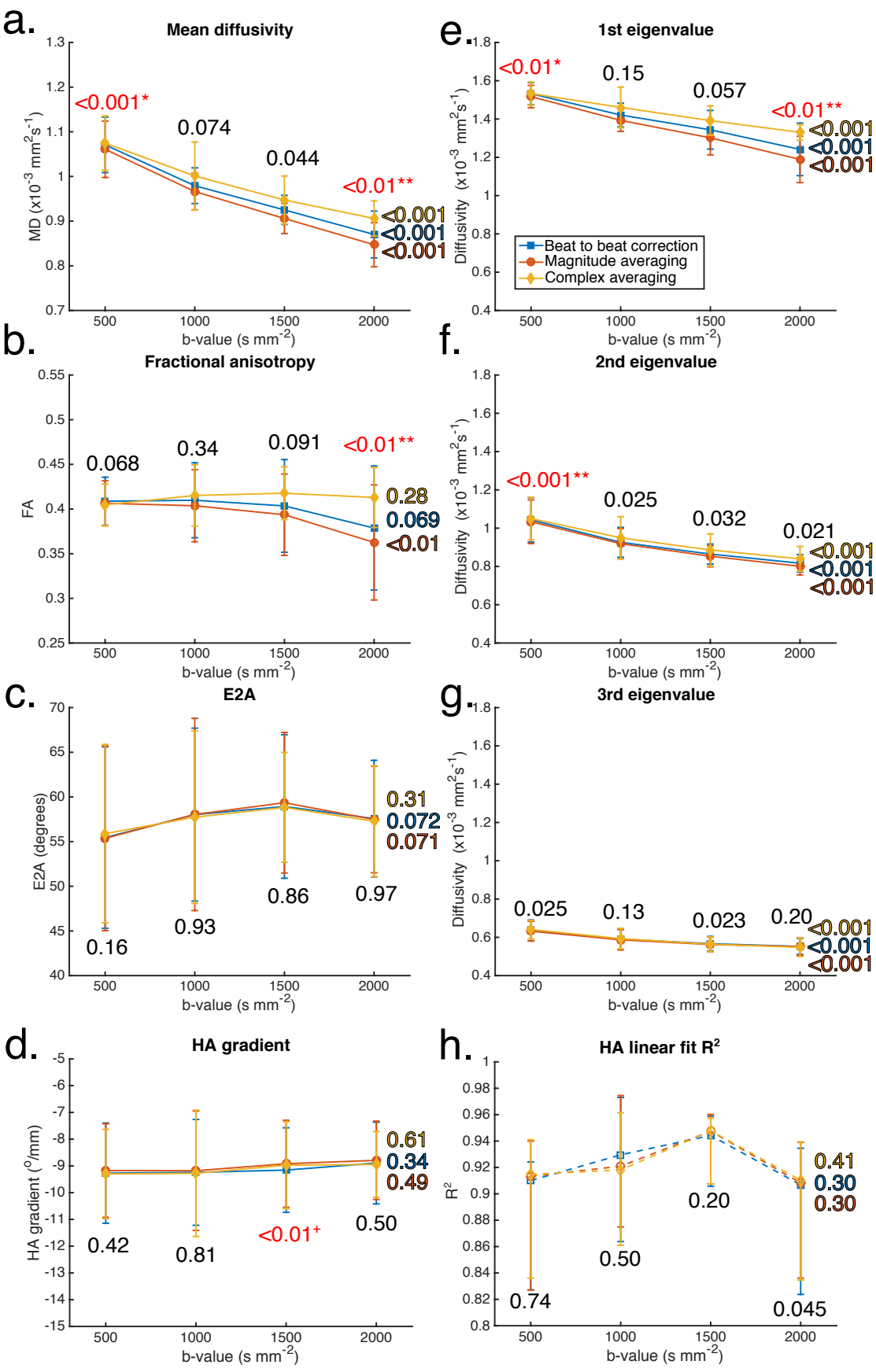

Figure 7: *In-vivo* results from all subjects using b_{ref}=34smm^{-2}. Data are plotted as mean ± standard deviation, except for the HA-R^2 which shows median ± interquartile

range. Results of one-way repeated-measures ANOVA tests (Friedman test for HA-R^2) between averaging methods at b_{main} are shown above each point. From the pairwise comparisons * indicates P≤0.01between complex and magnitude averaging, ** additionally indicates P≤0.01 between beat-to-beat corrected and magnitude averaged data. $^{+}$ indicates P≤0.01 between magnitude averaged and beat-to-beat corrected data. Results of one-way repeated measures ANOVA between b_{main} values for each method are shown at the end of each line.